Networks and Heterogeneous Media

https://www.aimspress.com/journal/nhm

NHM, 19(2): 822–841.
DOI: 10.3934/nhm.2024037
Received: 15 May 2024
Revised: 12 August 2024
Accepted: 19 August 2024
Published: 22 August 2024

Research article

Estimation of NO_x and O_3 reduction by dissipating traffic waves

Maya Briani[1], Rosanna Manzo[2], Benedetto Piccoli[3,*] and Luigi Rarità[4]

[1] Consiglio Nazionale delle Ricerche, Istituto per le Applicazioni del Calcolo "Mauro Picone", Via dei Taurini, 19, Rome, 00185, Italy

[2] Dipartimento di Scienze Politiche e della Comunicazione, University of Salerno, Via Giovanni Paolo II, 132, Fisciano (SA), 84084, Italy

[3] Department of Mathematical Sciences, Rutgers University-Camden, 311 N. Fifth Street, Camden, New Jersey, USA

[4] Dipartimento di Scienze Aziendali-Management & Information Systems, University of Salerno, Via Giovanni Paolo II, 132, Fisciano (SA), 84084, Italy

* **Correspondence:** Email: piccoli@camden.rutgers.edu; Tel: (856) 225-6356.

Abstract: Current research directions indicate that vehicles with autonomous capabilities will increase in traffic contexts. Starting from data analyzed in R. E. Stern et al. (2018), this paper shows the benefits due to the traffic control exerted by a unique autonomous vehicle circulating on a ring track with more than 20 human-driven vehicles. Considering different traffic experiments with high stop-and-go waves and using a general microscopic model for emissions, it was first proved that emissions reduces by about 25%. Then, concentrations for pollutants at street level were found by solving numerically a system of differential equations with source terms derived from the emission model. The results outline that ozone and nitrogen oxides can decrease, depending on the analyzed experiment, by about 10% and 30%, respectively. Such findings suggest possible management strategies for traffic control, with emphasis on the environmental impact for vehicular flows.

Keywords: road traffic modeling; traffic waves; emissions; Nitrogen oxides; ozone production

1. Introduction

Current scenarios of car traffic foresee the presence of vehicles with control capabilities. autonomous vehicles (AVs) are useful to mitigate traffic phenomena due to human habits, with consequent improvement of driving patterns and fuel consumption for traffic flows [1], as well as emissions [2], and effects on the environment and human health. Indeed, AVs on roads could lead to meaningful phenomena in terms of vehicles ownership, alterations in land use, travel demands, and

mode choice, see for instance [3]. Focusing on such possible effects, this study aims to show how a small number of AVs can mitigate the instabilities of traffic flow. In particular, this paper investigates the possible decrease of vehicle emissions and concentrations for pollutants at street level in traffic experiments in the presence of AVs. Some estimates of traffic emissions are first obtained from a microscopic model and traffic data of [1]. Then, concentrations of principal chemical species, i.e., ozone and nitrogen oxides, are evaluated by a system of differential equations with source terms resulting from traffic emissions. The analysis is done through mathematical models coupled with experimental data and shows how AVs bring benefits to the whole traffic system. .

1.1. Related works

Congestion waves often occur on road networks, see the experiments of [4] and [5]. In [1] and [6], this is explained from the human driving point of view, with negative effects for fuel consumption and the formation of traffic jams. In order to mitigate phenomena due to congestion, AVs have been widely considered [7], without analyzing real vehicle data or the effects of emissions. On the other hand, in [8] speed limits for the improvement of traffic and decrease of emissions have been studied. Indeed, for the improvement of traffic flow, there are various aspects to consider, such as: an increment of the combustion engine efficiency [9]; the adoption of hybrid vehicles [10]; and optimal routing and control on road networks [11]. Other aspects deal with emission variations due to AVs. In particular, vehicle emissions are sources of greenhouse gases that contribute to high climate changes [12] and stop-and-go waves [13], with consequent traffic instabilities. Models for traffic emissions have been widely studied [14], considering that estimations from real measurements [15] imply high costs. Emissions models provide information about the concentrations of various pollutants (nitrogen oxides, carbon monoxide and dioxide, hydrocarbons) that lead to the production of ozone. Estimations for emissions consider aggregate and microscopic models. The latter (see, for instance, [16–18]) focus on environmental impacts by using inputs such as the velocities of vehicles and the distance between them. The former use instantaneous measurements for vehicles. In this paper, emissions estimates are found through the model described in [19]. The difference with [2] is that the latter estimates emissions from a vehicle-specific power (VSP) analysis done in MOVES (motor vehicle emissions model) as follows: for vehicles in a traffic fleet, the emissions are a combination of velocities, accelerations, and their powers, with parameters tuned for nitrogen oxides of cars having internal combustion engines. Notice that our analysis for emissions deals only with real data, unlike other cases where simulations are used [20]. Finally, from emissions, the concentration of pollutants are obtained as in [21–23].

1.2. Main contributions and outline

The main contribution of the work is as follows. For various traffic experiments, first described in [1], a general microscopic model allows us to prove that emissions, in a traffic fleet travelling on a ring road, decrease in the presence of designed control algorithms managed by a unique AV. Then, focusing on a system of differential equations for chemical species, concentrations of pollutants at street level are numerically found. Meaningful decreases occur for concentrations of ozone and nitrogen oxides. Fuel consumption also follows this reductions, see [1]. In this case, the main point is to couple an emission estimation approach with chemical reaction models: the outcome is the estimation of the concentration of chemical compounds produced by traffic emissions in the atmosphere. This represents the novelty

of the proposal: the possibility of defining concentrations at ground level for the principal pollutants that are involved in ozone production. The main difference with other analyses, see [1] and [2], is the definition of a model that, starting from real measurements, allows estimations of the chemical species that define the dynamics in the atmosphere. The novelty of the paper is the evaluation of the concentrations at ground level for the principal pollutants that are involved in ozone production and the analysis of the effects on pollution of control strategies, implemented on the unique AV of the fleet in consideration. Such strategies show how possible reductions of pollutants are possible.

The paper is organized as follows. Section 2 deals with the contexts in which stop-and-go waves occur, with reference to the experimental scenarios for the analysis. Section 3 considers the model for emissions estimates and the systems of differential equations for the concentration of pollutants at street level. Finally, Section 5 presents numerical results. The paper ends with conclusions in Section 6.

2. Methodology

In this section, we briefly present the context in which stop-and-go waves develop and are then dampened by controlling a unique vehicle in designed traffic experiments. First, we consider the experimental setup and then the wave dampening controllers.

2.1. Design of the experiments

The vehicle emissions that are considered in this work are estimated from trajectories in the experiments analyzed in [1], based on the ring road experimental design of [4] and [5]. In this case, possible advantages are the absence of merging lanes and intersections that could make the analysis of traffic waves more difficult. The resulting captured traffic data frames the phenomenon of stop-and-go waves due to human driving behavior and the dampening effect occurred in presence of an AV.

The experiments, that follow the setup presented in [4], consist of 21 or 22 vehicles driving on a single-lane circular track of 260 meter circumference, located in a parking lot in Tucson, Arizona. The experiments are recorded by a 360-degree panoramic camera that is at the center of the ring road. Video recordings allow us to extract data for vehicle trajectories through computer vision algorithms, see [6] for details. When each experiment starts, vehicles are uniformly placed on the ring road, and the pilots are asked to drive as they would in usual traffic, and to follow the vehicle in front of them in safety conditions. In each experiment, there is a unique cognitive and autonomous test (CAT) Vehicle, that is either human-controlled or autonomous. In particular, the CAT vehicle begins under a control managed by the pilot, who follows the same instructions of all other drivers. When stop-and-go waves occur, the CAT vehicle is switched into an autonomous driving mode (Experiments A and C) or is still controlled by the human driver, who is asked to drive at a wished velocity (Experiment B). The experiments prove that stop-and-go waves are dampened or vanish through the control of a unique vehicle on the ring road.

In short, the procedure has the following steps for each possible experiment: set uniformly spaced vehicles on the track; drive with all human-controlled vehicles; ask the driver of the CAT vehicle to set up the autonomous driving (Experiments A and C) or to change the driving velocity (Experiment B); disable the control strategy; end experiment, all vehicles stop.

The features of Experiments A, B, and C depend on how the CAT vehicle is controlled.

2.2. Controllers for traffic waves

This subsection briefly presents the velocity controllers implemented on the CAT vehicle to stabilize traffic conditions on the ring road. As the strategy is to command the autonomous vehicle to drive uniformly and safely with a defined velocity, an equilibrium condition, see [24], occurs for the overall traffic flow.

The basic idea for the structure of the controllers is as follows. A *commanded velocity* is defined as $v^{cmd}(t) = F\left(v^{AV}(t), v^{lead}(t), U(t)\right)$, where $F(\cdot)$ is a given function of $v^{AV}(t)$, the velocity of the CAT vehicle; $v^{lead}(t)$, the velocity of the vehicle ahead of the CAT and establishes the gap Δx, i.e., the distance from the front bumper of the CAT vehicle to the rear bumper of the lead one; and $U(t)$, a *desired velocity* that, if chosen correctly through suitable strategies, stabilizes traffic flows and reduces traffic waves. The velocity $v^{cmd}(t)$ is then the input of a low-level controller on the CAT vehicle and the output is the actuation of the brake or accelerator. In what follows, we describe the controllers implemented on the CAT vehicle, precisely: the *FollowerStopper* controller (Experiment A); the human-implemented control (Experiment B); the proportional integral (PI) with saturation controller (Experiment C).

Experiment A (FollowerStopper controller)
In this case, the controller commands exactly $U(t)$ (estimated by a human observing the experiment) whenever safe but commands $v^{cmd}(t) < U(t)$ whenever safety is needed, possibly considering $v^{lead}(t)$. From $v^{AV}(t)$, $v^{lead}(t)$, and Δx, three regions that allow a safe velocity for the autonomous vehicle, are defined: (i) a safe region where $v^{cmd}(t) = U(t)$, (ii) a stopping region where $v^{cmd}(t) = 0$, and (iii) an adaptation region where $v^{cmd}(t)$ is an average of $v^{lead}(t)$ and $U(t)$.

Experiment B (traffic control via a trained human driver)
For Experiment B, a trained human pilot is asked to maintain a certain speed and slow down only in case of collisions with the vehicle ahead. The desired speed, determined externally by the staff who observes the experiment and communicated to the driver through a two-way radio, is obtained as the circumference of the ring road divided by the time the CAT vehicle needs to make a complete pass around the ring road.

Experiment C (a PI controller with saturation)
The CAT vehicle estimates the average speed $\overline{v}(t)$ of the vehicles in front, and drive as close to such speed in safety conditions. For the autonomous vehicle, the controller tracks $v^{cmd}(t)$ by a standard proportional integral (PI) control logic where the error signal is the deviation from $\overline{v}(t)$. The controller also includes a saturation effect, in which the CAT vehicle should command $v^{lead}(t)$ for safety reasons when Δx is small.

3. Emissions and pollutants estimations

In this section, we consider the estimation of emissions and pollutants production on the ring track due to the vehicular traffic. In our case, as we deal with high amounts of UV radiations and heavy vehicular flows, we focus on nitrogen oxides (NO_x) emissions that generate ozone (O_3). Indeed, there is a mix of effects because NO_x is also due to vehicle exhaust while UV rays hit the oxygen molecules in

the air and provoke chemical reactions that produce the ozone. Hence, O_3, besides its dangerous effects on the human health [25,26], is the result of chemical dynamics in sunlight environments [27,28]. First, we shortly describe a microscopic model that, starting from velocities and accelerations of vehicles in Experiments A, B, and C, estimates the emissions on the ring track. Then, we consider the main reactions of NO_x for the production of ozone, whose evolution obeys a system of ordinary differential equations.

3.1. Emissions model

We deal with the microscopic emissions model discussed in [19]. Consider a vehicle k that, at time t, moves at speed $v_k(t)$ [m/s] and is subject to an acceleration $a_k(t)$ [m/s^2]. Define the vectors:

$$\omega_k(t) := \left(1,\ v_k(t),\ v_k^2(t),\ a_k(t),\ a_k^2(t),\ v_k(t)\,a_k(t)\right),$$

$$\varphi := (f_1,\ f_2,\ f_3,\ f_4,\ f_5,\ f_6),$$

where the constants f_i, $i = 1, ..., 6$, are associated to NO_x emissions for a petrol car and are listed in Table 1. For other types of coefficients, as well as different pollutants and categories of vehicles, we refer the reader to [19].

Table 1. NO_x parameters for an internal combustion engine car, where g indicates grams.

Condition	f_1 $[\frac{g}{s}]$	f_2 $[\frac{g}{m}]$	f_3 $[\frac{g\,s}{m^2}]$	f_4 $[\frac{g\,s}{m}]$	f_5 $[\frac{g\,s^3}{m^2}]$	f_6 $[\frac{g\,s^2}{m^2}]$
$a_k(t) \geq -0.5$	6.19e−04	8e−05	−4.03e−06	−4.13e−04	3.80e−04	1.77e−04
$a_k(t) < -0.5$	2.17e−04	0	0	0	0	0

The emissions of the vehicle k are estimated as:

$$E_k(t) = \max\left\{E_0,\ \omega_k(t)\cdot\varphi^T\right\}, \tag{3.1}$$

where E_0 is an emission lower-bound, that is assumed zero when using f_i, $i = 1, ..., 6$, of Table 1. Finally, the total emissions $E(t)$ for a set of N travelling vehicles is:

$$E(t) = \sum_{k=1}^{N} E_k(t). \tag{3.2}$$

Remark 1. *Most microscopic emissions models deal with combinations of polynomial expressions in velocities and accelerations, see for instance [29]. Hence, our approach for emissions can easily be adapted to other models.*

3.2. Chemical reactions and the production of O_3

We now consider the chemical reactions for NO_x gases and the production of O_3. For car engines, when combustion phenomena interest hydrocarbons at high temperatures, NO_x emissions are due to nitrogen (N_2) and oxygen (O_2). The formation of O_3 is described as follows via the contributions of nitrogen monoxide (NO), nitrogen dioxide (NO_2), and atomic oxygen (O).

Assume that h and ν are, respectively, the Planck's constant and its frequency. For fixed reaction rate constants k_1, k_2, and k_3, we get the reactions [30, 31]:

$$N_2 + O_2 \to 2NO, \tag{3.3}$$

$$2NO + O_2 \to 2NO_2, \tag{3.4}$$

$$NO_2 + h\nu \xrightarrow{k_1} O + NO, \tag{3.5}$$

$$O + O_2 + M \xrightarrow{k_2} O_3 + M, \tag{3.6}$$

$$O_3 + NO \xrightarrow{k_3} O_2 + NO_2, \tag{3.7}$$

where M is either N_2 or O_2 for the absorption of the energy excess in Eq (3.6).

Notice that NO is produced by the reaction in Eq (3.3). In the combustion phenomenon, Eq (3.4) indicates the formation of NO_2 that can be photo-dissociated into O, as described by Eq (3.5). This last step is fundamental for the formation of tropospheric ozone [32]. Precisely, Eq (3.6) provides O_3 that, following the reaction in Eq (3.7), is destroyed and transformed into O_2 and NO_2. Hence, the reactions in Eqs (3.6) and (3.7) do not produce net ozone, as there is only a recycling of O_3 and NO_2. Net ozone is produced only when the atmosphere contains other possible pollutants, i.e., carbon monoxide and methane, for instance. In this work, we consider only the reactions in (3.5), (3.6), and (3.7) for the whole ground-level ozone formation.

Remark 2. *For the emissions of vehicles, NO_2 has a maximum concentration for medium engine speed (from* 300 *to* 1000 *revolutions per minute, rpm) and low engine speed (from* 80 *to* 300 *rpm). For high speeds (from* 1000 *to* 4000 *rpm), NO_2 emissions usually become less than 4% ([33]). In what follows, considering the recent analysis in [34], for our numerical studies, we will use a NO_2 concentration equal to 15% of NO_x.*

For each reaction, an ordinary differential equation (ODE) is defined and then used to get the final system for the ozone production due to traffic emissions (further remarks are in [22]).

Indicate by $[\cdot] = [\text{weight unit/volume unit}]$ the chemical species concentration, and denote by $\Gamma(t) = (\Gamma_1(t), \Gamma_2(t), \Gamma_3(t), \Gamma_4(t), \Gamma_5(t))$ the vector with $\Gamma_1(t) = [O]$, $\Gamma_2(t) = [O_2]$, $\Gamma_3(t) = [O_3]$, $\Gamma_4(t) = [NO]$, and $\Gamma_5(t) = [NO_2]$. Assume that the reactions occur in a volume of dimension Δx^3 and the traffic total emission is a source term for Γ_4 and Γ_5. The overall variation of NO_x concentration in Δx^3 is as follows at each time t:

$$S(t) := \frac{E(t)}{\Delta x^3}, \tag{3.8}$$

where $E(t)$ obeys (3.2). Omitting for simplicity the dependence on the time t, the final system is:

$$\begin{cases} \Gamma_1' = -k_2\Gamma_1\Gamma_2^2 + k_1\Gamma_5, \\ \Gamma_2' = -k_2\Gamma_1\Gamma_2^2 + k_3\Gamma_3\Gamma_4, \\ \Gamma_3' = k_2\Gamma_1\Gamma_2^2 - k_3\Gamma_3\Gamma_4, \\ \Gamma_4' = k_1\Gamma_5 - k_3\Gamma_3\Gamma_4 + (1-p)S, \\ \Gamma_5' = -k_1\Gamma_5 + k_3\Gamma_3\Gamma_4 + pS, \end{cases} \tag{3.9}$$

where $p = 0.15$ corresponds to 15% of NO_2 (see Remark 2) and the constant kinetic rates k_1, k_2, and k_3 are estimated in [35] and shown in Table 2.

Table 2. Values of k_1, k_2, and k_3, where *molecule* is the number of molecules.

Kinetic rates	Value
k_1	$0.02\ s^{-1}$
k_2	$6.09e-34\ cm^6\ molecule^{-2}\ s^{-1}$
k_3	$1.81e-14\ cm^3\ molecule^{-1}\ s^{-1}$

The rate of change for concentrations in non-linear systems such as (3.9) has a high degree of stiffness. Hence, for possible numerical treatments, some adapting techniques for time step sizes are necessary to avoid instabilities and increments of computational work. Various approaches exist to face such numerical problems. In this work, system (3.9) is solved via the MATLAB tool *ode23s*, which uses an adaptive step size and works by an implicit Runge-Kutta method based on the Rosenbrock formula of order 2. The temporal refinement technique defines either large or small time steps, respectively, for slow and fast varying components, and intermediate time values that are not always available. In particular, in system (3.9), the source term S, which depends on the emissions (3.2), needs a suitable attention as it is defined on a time scale, that is larger than the one of reactions dynamics. Hence, possible intermediate time values might always be required. If they are not directly available, they have to be computed by a high-order interpolation, which does not affect the order of the method. Precise details are carefully addressed in [21, 23, 36].

4. On coupling traffic with emissions and chemical reaction models

In this section, we briefly discuss the mathematical theory for coupled traffic, emissions and atmospheric models.

Traffic models are mostly cast at two different scales: microscopic and macroscopic. The former is expressed by a collection of ODEs of the type:

$$\dot{v}_i = F_i(x_{i+1}, x_i, v_{i+1}, v_i), \tag{4.1}$$

where (x_i, v_i) is the position-velocity vector of the i-th car on the road, and F_i describes the acceleration. We refer the reader to [37].

At the macroscopic level, traffic is described by partial differential equations, mostly hyperbolic ones, such as

$$u_t + f(u)_x = h(u), \tag{4.2}$$

where u is the vector of considered macroscopic quantities, e.g., density and modified momentum, f is the flux function, and h a source term. A complete discussion of such equations is beyond the scope of this paper, but we point out the most commonly used model, the Lighthill-Whitham-Richards model [38, 39], consisting of a single conservation law:

$$\rho_t + (v(\rho)\rho)_x = 0, \tag{4.3}$$

where $\rho \in [0, \rho_{max}]$ is the density of the cars and $v(\rho)$ is the average speed, assumed to depend only on the density. For more discussion, see [37].

Emissions models as (3.1) can be paired to microscopic models directly using the data (x_i, v_i) from (4.1) and computing the accelerations a_i of the i-th vehicle. The result of the emissions model can then be directly fed into the system of ODEs (3.9). From a mathematical point of view, the models are weakly coupled, with the emissions model depending on the input of the traffic model, and the chemical model depending on the input of the emissions model. We, thus, immediately have the following:

Proposition 1. *Consider the system given by Eq* (4.1) *with N vehicles, i.e.,* $i = 1, \dots, N$. *Assume that there exists a bounded set* $A \subset \mathbb{R}^{2N}$ *such that any solution with initial datum* $((x_{1,0}, v_{1,0}), \dots (x_{N,0}, v_{N,0}))$ *remains in A for all times* $t \geq 0$, *and that* F_i *are Lipschitz continuous in A. Then, for every initial datum for the system* (4.1), (3.1), *and* (3.9), *with position-velocity vectors in A, there exists a unique solution depending continuously on the initial datum.*

Proof. Given an initial datum with position-velocity vectors in A, there exists a solution to the system (4.1) due to the assumptions on F_i. Then the solution can be used as the input to the system (3.1) generating an emission signal $E(t)$. The latter can be used as the input to the system (3.9). For the system (3.9), notice that $\Gamma_4' + \Gamma_5' = S(t)$. Since the solution to (4.1) is bounded, we deduce that $E(t)$ is bounded, thus $S(t)$ is bounded. We have that both Γ_4 and Γ_5 remain bounded. Therefore, the whole vector $\Gamma(t)$ remains bounded for all times. Due to the Lipschitz continuity of F_i on A and the right-hand side of (3.9) on bounded regions, we conclude. □

Remark 3. *We point out that the assumption on the existence of the region A is a minor limitation. Indeed, most commonly used models, such as the follow-the-leader, the optimal velocity, and (modifications) of the intelligent driver models do satisfy such assumptions. We refer the reader to [37] and [40] for details.*

Emissions models as (3.1) can be also paired to macroscopic models of the type (4.2), as long as an acceleration signal $a(t, x)$ can be computed. This can not be done directly for models with two equations, see [41]. However, there exist models for fuel consumption directly using (4.3), see [42].

This, in turn, allows us to also estimate emissions. As before, the emissions model can be used to produce an input for the system of ODEs (3.9). The overall system consists of a system of PDEs (4.2) providing input to the emission model (3.1), which in turn provides an input the ODE system (3.9).

Even more, one can pair to diffusion-reaction model for the chemical species as done in [22] and [23]. Such systems can be analyzed by combining tools for conservation laws with those for parabolic equations. We refer the reader to [43] for a general result on the coupling of hyperbolic and parabolic models, which includes the system (4.3)-(3.1)-(3.9) as a special case.

5. Numerical tests

This section deals with results based on Experiments A, B, and C, all interested in time phases of autonomy and human control driving. The main features of the experiments, described in detail in [1] and [2], are as follows.

At the beginning of Experiment A, the CAT vehicle is controlled by the human driver. During the experiment, the first traffic wave appears at 79 s. The wave-dampening controller of type *FollowerStopper* becomes active at 126 s, and set with $U = 6.50$ m/s. Then, U is varied step by step to test how traffic conditions vary. At 463 s, the autonomy of the CAT vehicle is disabled. The experiment ends at 567 s.

Experiment B has similar features. The first traffic wave occurs at 55 s from the beginning of the experiment. The CAT vehicle driver is asked to drive with $U = 6.25$ m/s at 112 s. Also in this case, the velocity U varies step by step. The end of the experiment is at 409 s.

For Experiment C, the traffic wave appears at 161 s. The PI controller with saturation becomes active at 218 s and remains so until 413 s (the end of the experiment). In this case, U varies continuously as it is completely determined by the controller at each time instant.

Table 3 summarizes all phases of each experiment: a traffic initial phase, IPH; a time interval, SGW, with stop-and-go waves; various autonomy phases, indicated by AUT_i; an interval with no autonomy, NA.

Table 3. Summary of the main features for Experiments A, B, and C.

Experiment	A	B	C
Start	IPH = [0, 79[s	IPH = [0, 55[s	IPH = [0, 161[s
Waves	SGW = [79, 126[s	SGW = [55, 112[s	SGW = [161, 218[s
Autonomy	AUT_1 = [126, 222[s, $U = 6.50$ m/s AUT_2 = [222, 292[s, $U = 7.00$ m/s AUT_3 = [292, 347[s, $U = 7.50$ m/s AUT_4 = [347, 415[s, $U = 8.00$ m/s AUT_5 = [415, 463[s, $U = 7.50$ m/s	AUT_1 = [112, 202[s, $U = 6.25$ m/s AUT_2 = [202, 300[s, $U = 7.15$ m/s	AUT_1 = [218, 413] s
No Autonomy	NA = [463, 567] s	NA = [300, 409] s	-

The contents of this section are the following: First, we discuss the results due to NO_x emissions, and then, we examine how pollutants vary according to the different time phases in the considered experiments.

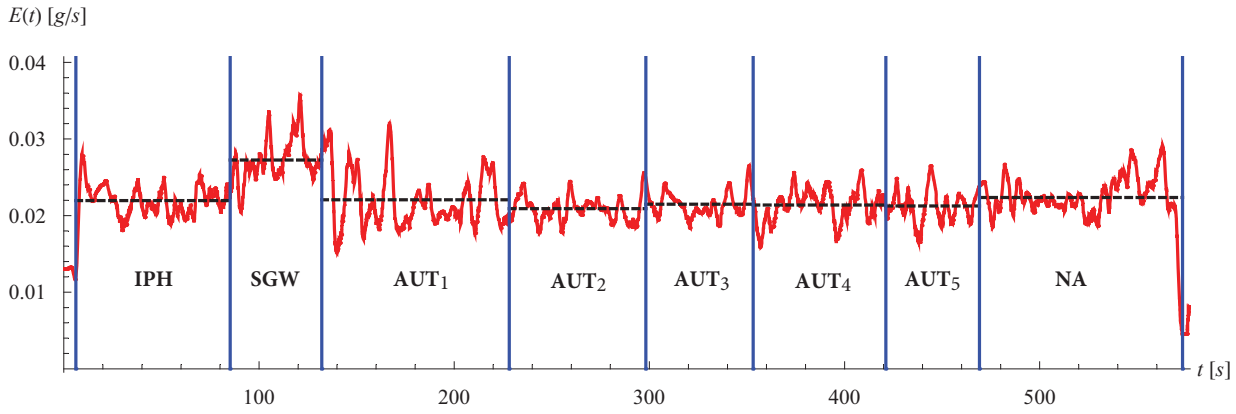

Figure 1. $E(t)$ for Experiment A (red line), and the average values in intervals (dashed black lines).

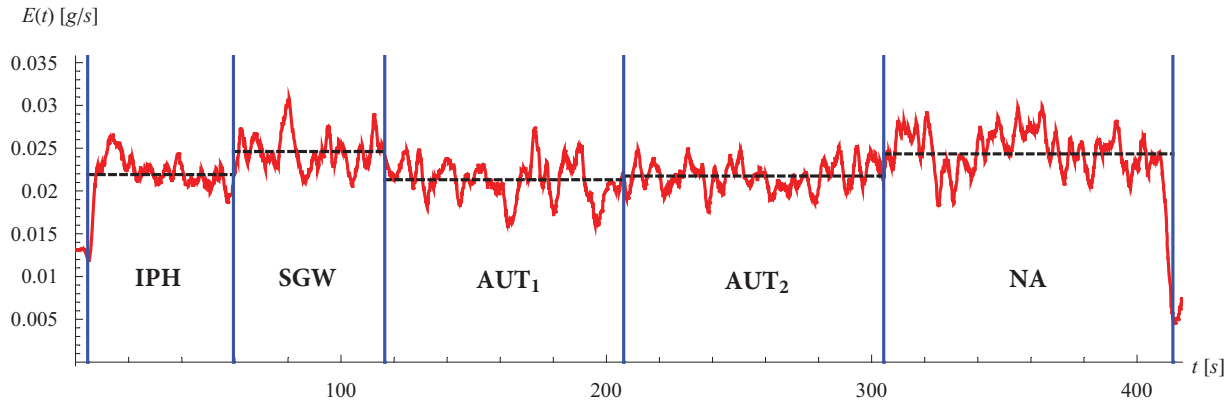

Figure 2. $E(t)$ for Experiment B (red line), and the average values in intervals (dashed black lines).

5.1. Estimating NO_x emissions for the experiments

In order to estimate the NO_x emissions of the vehicle fleet in the described experiments, we show the evolution of $E(t)$, see Eq (3.2), in Figures 1–3. For the time intervals of type SGW, the average NO_x emissions for Experiments A, B, and C are, respectively: 27.2514 mg/s, 24.6108 mg/s, and 28.7677 mg/s. Values for cases A and C are comparable, hence indicating that the experiments have the same features before the activation of possible control strategies.

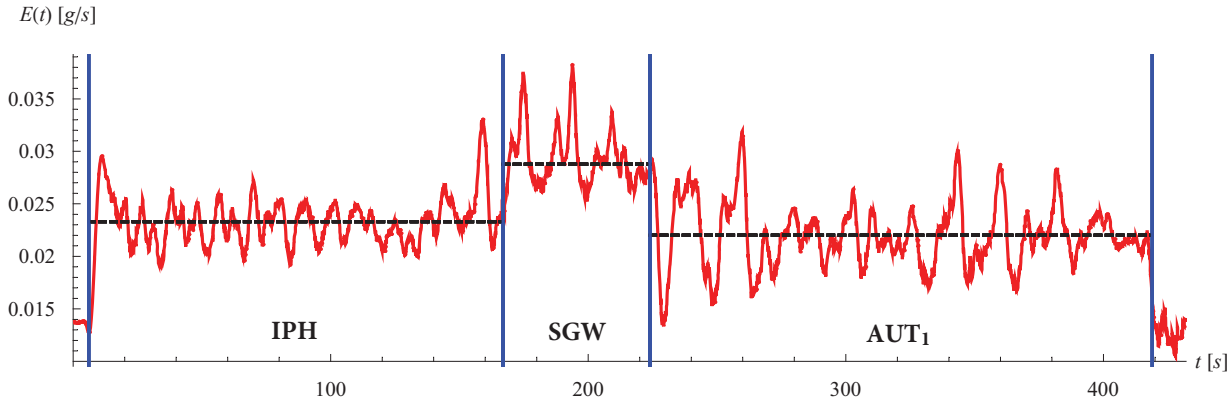

Figure 3. $E(t)$ for Experiment C (red line), and the average values in intervals (dashed black lines).

For Experiment A, in AUT_1, the wave is almost dampened but not removed completely. When $U = 7.00$ m/s in AUT_2, the CAT vehicle moves at a speed almost similar to the average traffic one, leading to the lowest average NO_x emissions in the experiment. When the FollowerStopper controller is deactivated in the interval NA, the traffic wave appears again and the average NO_x emissions increases at a value similar to the one obtained in AUT_1. For all time intervals, Table 4 provides the various NO_x emissions average values, expressed in milligrams/second [mg/s] and grams/minute [g/min], for Experiment A.

Table 4. Experiment A: Average NO_x emissions (AEs) for different time intervals (TIs).

TIs [s]	AEs [mg/s]	AEs [g/min]
IPH	21.9647	1.317882
SGW	27.2514	1.635084
AUT_1	22.0546	1.323276
AUT_2	20.9003	1.254018
AUT_3	21.4913	1.289476
AUT_4	21.3764	1.282584
AUT_5	21.2476	1.274856
DA	22.3701	1.342206

For Experiment B, in AUT_1, the CAT vehicle operator starts driving with $U = 6.25$ m/s, the traffic wave is damped, and the average emission decreases. However, when U is increased to 7.15 m/s (in AUT_2), the overall traffic on the ring track becomes more regular as the average speed of the vehicle fleet is similar to the one of the CAT vehicle. In this case, the differences between the average NO_x emissions in AUT_1 and AUT_2 are not very meaningful. In the interval NA, the human control ends, the stop-and-go wave occurs again, and the average NO_x emission increases. Table 5 presents the average NO_x emissions, in terms of milligrams/second [mg/s] and grams/minute [g/min], for Experiment B for all time intervals.

Table 5. Experiment B: Average NO_x emissions (AEs) for different time intervals (TIs).

TIs [s]	AEs [mg/s]	AEs [g/min]
IPH	21.9185	1.315110
SGW	24.6108	1.476648
AUT_1	21.3137	1.278822
AUT_2	21.7398	1.304268
DA	24.3413	1.460478

In the case of Experiment C, the first strong wave appears at the beginning of the interval SGW. The PI controller with saturation becomes active in AUT_1, the wave is reduced, and the average NO_x emissions decrease. In this case, the control strategy uses data measured by the CAT vehicle itself, and no additional external information is needed. Hence, unlike Experiment A, the wave dampening is different, and the emissions rate is quite irregular. Table 6 shows the average NO_x emissions values (in milligrams/second [mg/s] and grams/minute [g/min]) for Experiment C in all time intervals.

Table 6. Experiment C: Average NO_x emissions (AEs) for different time intervals (TIs).

TIs [s]	AEs [mg/s]	AEs [g/min]
IPH	23.3101	1.398606
SGW	28.7677	1.726062
AUT_1	22.0067	1.320402

Notice that the presence of a unique autonomous vehicle allows a total reorganization of traffic dynamics. For all experiments, this is also evident from the percent reduction in NO_x emissions, evaluated in periods with waves and autonomy phases. The obtained results are in Table 7 (second column), which shows how Experiments A and C are similar in terms of traffic control, unlike Experiment B, which deals with a trained human driver. Table 7 also shows, in the third column, a comparison with the reductions described in [2] in the case of the experiment fleet under consideration. The evident differences with our approach are due to a different model for emissions: in [2], the estimation is analyzed via the motor vehicle emissions model (MOVES), which considers various factors, such as humidity and temperature, road links, the vehicle fleet mix and age distribution, as well as the vehicle-specific power (VSP) distribution.

Table 7. Percent reduction in emissions.

Experiment	% reduction	% reduction in [2]
A	23.3	73.5
B	11.7	60.8
C	23.5	63.3

5.2. Production of pollutants

The estimation of concentrations for pollutants along the ring track at street level are found by solving system (3.9). As the aim is to show concentration reductions due to autonomous vehicles, we consider separate analyses for experiment phases where stop-and-go waves occur (the CAT vehicle has a disabled control) and phases where autonomous driving dissipates the wave (CAT vehicle is exerting a control). To obtain the estimates, we solve numerically system (3.9) on a time interval $I = [0, T]$ by choosing source terms (3.8). To obtain simulations over a larger time horizon, we prolong the source term signal by repeating the emissions profile of the time interval I. In simple words, we consider a periodic emissions profile using data from the experiment in the corresponding phase (waves or autonomy). In order to discriminate among the traffic sources in different experiments for stop-and-go waves and autonomy phases, we adopt the following notations: $S_{X,Y}$ is the repetition of the source term for Experiment X, over I, of the time interval Y, where $X \in \{A, B, C\}$, identifies the experiment, and $Y \in \{SGW, AUT_i\}$, identifies the experiment phase. For all simulations, chemical species are computed for each volume of size Δx^3, with $\Delta x = \dfrac{C}{\pi}$, where $C = 260$ m is the length of the ring road. We fix $T = 30$ min and choose the following initial concentrations:

$$\Gamma_1(0) = \Gamma_3(0) = 0,\ \Gamma_2(0) = 5.02 \times 10^{18}\ \text{molecule/cm}^3,$$

$$\Gamma_4(0) = (1-p)\, S_{X,Y}(0)\,,\ \Gamma_5(0) = p S_{X,Y}(0)\,,$$

where $p = 0.15$.

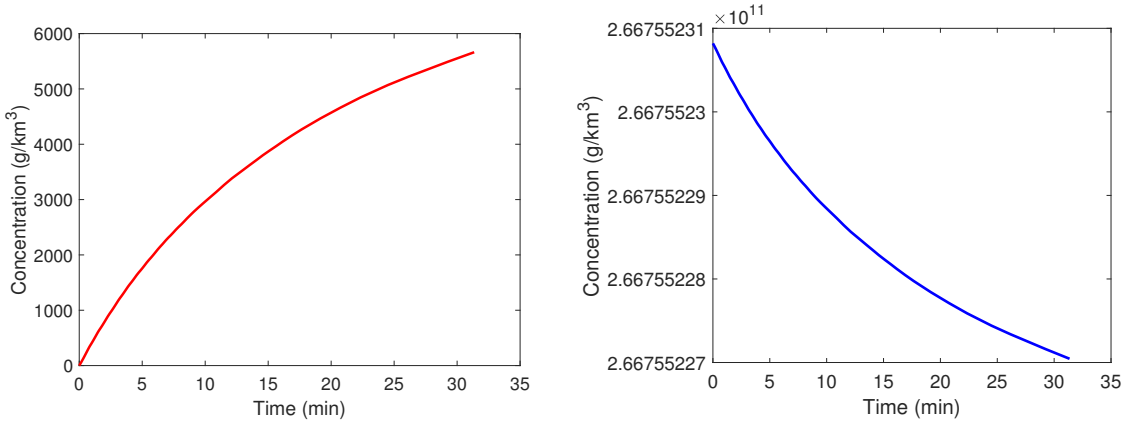

Figure 4. Time variation of the concentration (g/km^3) for O_3 (left) and O_2 (right) by solving (3.9) via $S_{A,SGW}$.

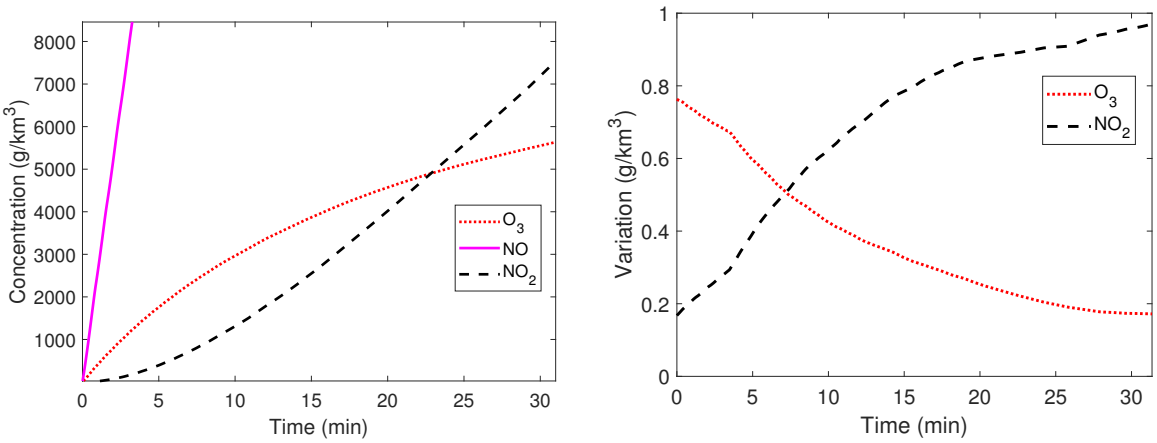

Figure 5. Left: Comparison between time variations of concentrations (g/km^3) for O_3 (point red), NO (violet), and NO_2 (dashed black). Right: Variation rates for O_3 (point red) and NO_2 (dashed black) by solving (3.9) via $S_{A,SGW}$.

For $S_{A,SGW}$ in (3.9), that is stop-and-go waves in Experiment A, we get Figures 4 and 5 for the principal pollutants at ground level. Precisely, in Figure 4, O_2 (right panel) remains almost constant, unlike O_3 (left panel) that increases rapidly. As expected, O_2 decays but the variation is insignificant, proving that the overall environment is governed by a vital gas. On the contrary, O_3 increases because stop-and-go waves create high oscillations in traffic. Similar situations occur in Figure 5 for NO and NO_2: indeed, NO grows much faster than NO_2, which, in turn, exceeds O_3 at about 23 min. The different evolution for the two types of nitrogen oxides is due to the nature of involved molecules: as the mono-atomic oxygen O is unstable, at ground level, NO tends to explode and then disappears, and this confirms its low toxicity for human health; on the contrary, NO_2 has a smoother dynamic due the stability of O_2. The variation rates of O_3 and NO_2 also show that the former tends to a steady state while the latter continues its growth. Other possible behaviors, related to vertical and/or horizontal diffusion and possible decays of the various pollutants, are described by different models and are here omitted. As

for the final values of the concentrations for O_3 and NO_2 at T, we have:

$$\Gamma_3(T) = 5.6633 \text{ kg/km}^3, \Gamma_5(T) = 7.6605 \text{ kg/km}^3,$$

while, from [1], the fuel consumption (FC) is, for the SGW interval of Experiment A:

$$\text{FC} = 24.1\ l/100 \text{ km}.$$

Table 8 reports the values of $\Gamma_3(T)$ and $\Gamma_5(T)$, obtained using source terms corresponding to S_{A,AUT_i}, $i = 1, ..., 5$, and the percentage of variations with respect to $S_{A,SGW}$. There is an overall decrease in the concentration of pollutants during the intervals of autonomy. In particular, the highest variations for O_3 and NO_2 are about 10% and 28%, respectively, in the best control period, AUT_2. For FC, the highest decrease is in AUT_3. Histograms in Figure 6 show the variation percentages for the principal pollutants and FC.

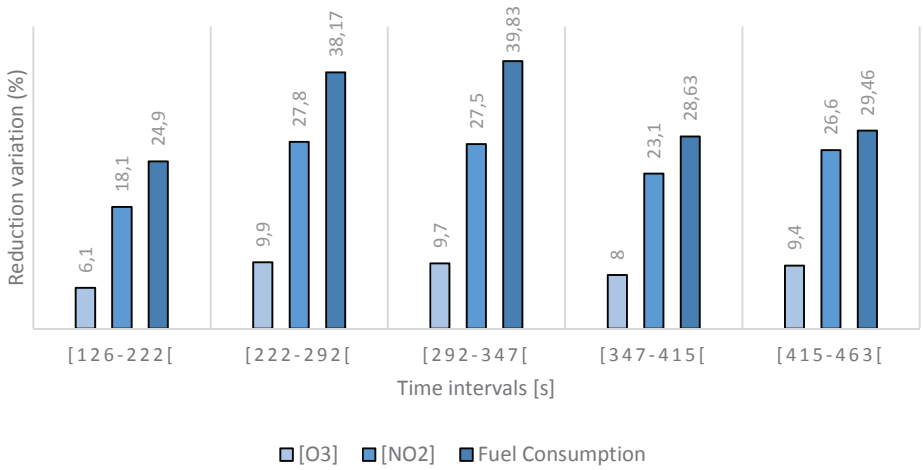

Figure 6. Histograms of variation percentages for O_3, NO_2, and FC by choosing different S_{A,AUT_i}.

Table 8. Concentrations (C) of O_3 and NO_2 at $T = 30$ for S_{A,AUT_i}, $i = 1, ..., 5$, and variations (V) with respect to $S_{A,SGW}$; FC in AUT_i and variations (VF) with respect to $S_{A,SGW}$.

Source term	C [kg/km^3]	V	FC [l/100 km]	VF
S_{A,AUT_1}	$\Gamma_3 = 5.3175$ $\Gamma_5 = 6.2709$	−6.1% −18.1%	18.1	−24.90%
S_{A,AUT_2}	$\Gamma_3 = 5.1022$ $\Gamma_5 = 5.5256$	−9.9% −27.8%	14.9	−38.17%
S_{A,AUT_3}	$\Gamma_3 = 5.1119$ $\Gamma_5 = 5.5578$	−9.7% −27.5%	14.5	−39.83%
S_{A,AUT_4}	$\Gamma_3 = 5.2098$ $\Gamma_5 = 5.8872$	−8.0% −23.1%	17.2	−28.63%
S_{A,AUT_5}	$\Gamma_3 = 5.1313$ $\Gamma_5 = 5.6191$	−9.4% −26.6%	17	−29.46%

For the experiments phases $S_{B,SGW}$ and S_{B,AUT_i}, $i = 1, 2$, using the corresponding source terms for (3.9), the concentrations of pollutants behave similarly. In particular, for $S_{B,SGW}$, we get:

$$\Gamma_3(T) = 5.4341 \text{ kg/km}^3, \Gamma_5(T) = 6.7110 \text{ kg/km}^3,$$

and, in the SGW phase for Experiment B, the fuel consumption is FC = 21.8 l/100 km. The decrease in pollutants and fuel consumption caused by autonomy are reported in Table 9. In this case, the best control period, AUT_2, shows the highest decreases of both pollutants O_3 and NO_2 and of fuel consumption. Histograms of Figure 7 present an overview for all types of variations.

Table 9. Concentrations (C) of O_3 and NO_2 at $T = 30$ for S_{B,AUT_i}, $i = 1, 2$, and variations (V) referred to $S_{B,SGW}$; FC in AUT_i and variations (VF) referred to the SGW interval of Experiment B.

Source term	C [kg/km^3]	V	FC [l/100 km]	VF
S_{B,AUT_1}	$\Gamma_3 = 5.3363$ $\Gamma_5 = 6.3371$	−1.8% −5.6%	17.8	−18.35%
S_{B,AUT_2}	$\Gamma_3 = 5.2798$ $\Gamma_5 = 6.1350$	−2.8% −8.6%	17.1	−21.56%

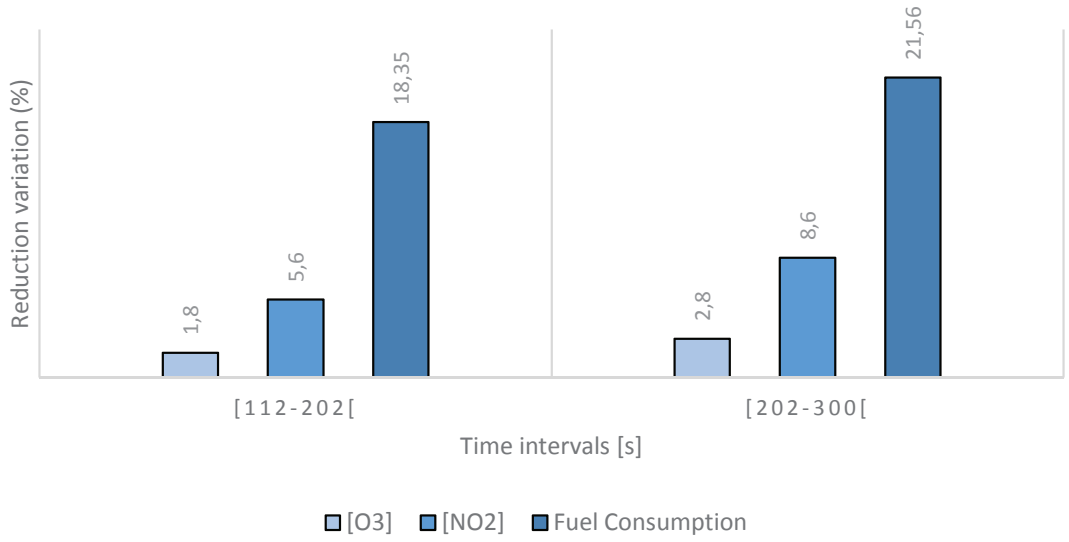

Figure 7. Histograms of variation percentages for O_3, NO_2, and FC for different choices of S_{B,AUT_i}.

Finally, we consider $S_{C,SGW}$ and S_{C,AUT_1} and the relative source terms for system (3.9). For $S_{C,SGW}$, we obtain:

$$\Gamma_3(T) = 5.7421 \text{ kg/km}^3, \Gamma_5(T) = 8.0181 \text{ kg/km}^3, \text{FC} = 26.3\ l/\ 100 \text{ km}.$$

When the controller is activated in AUT_1, we have:

$$\Gamma_3(T) = 5.5957 \text{ kg/km}^3, \Gamma_5(T) = 7.3684 \text{ kg/km}^3, \text{FC} = 20.27\ l/100 \text{ km}.$$

Hence, autonomy is able to decrease the concentrations of O_3 and NO_2 by 2.5% and 8.1%, respectively, while fuel consumption is reduced by 21.3%.

For Experiments A, B and C, Table 10 shows comparisons among the final values of concentration for O_3 and NO_2 in SGW and in the best autonomy phases. For O_3, the variation is about –10% in Experiment A, while for Experiment B and C is almost similar (about –3%). Indeed, Experiments B and C show a variation of approximately one-third of the one obtained with Experiment A. The same happens with NO_2 with different percentage values: about –30% for Experiment A and between –8% and –8.5% for Experiments B and C. We conclude that the control strategy, implemented in the three different experiments, deeply influences the variations of pollutants. Experiment A presents the highest decrease rates and therefore the use of autonomous vehicles, which are controlled by an external input communicated by an infrastructure (control design of type FollowerStopper), highlights the better results in terms of traffic regularity. The use of simple communications to the driver in Experiment B (control design of type *trained human driver*) indicates a possible decrease but the human component alone is not sufficient to guarantee very high performances in terms of the reduction of pollutants. Similar effects are also obtained by using control strategies based on local information (Experiment C, control design of type *PI controller with saturation*). This last case indicates recorded NO_2 levels that are quite higher than those detected in other experiments, thus showing that the results may depend on the specific experiment conditions.

In conclusion, the control with infrastructure communication achieved the best performance, while the one with a human actuator or local controller had a minor effect, but still significant. The overall recommendation would be to use the first controller whenever possible, resorting to the other two when the first is not available.

Table 10. Concentrations of O_3 and NO_2 at $T = 30$ in SGW ($\mathbf{C}_{SGW}$) and in the best autonomy phase ($\mathbf{C}_{AUT,best}$) for each experiment; variations (V) between the concentrations in the different time intervals.

Experiment	$\mathbf{C}_{SGW}$ **[kg/km^3]**	$\mathbf{C}_{AUT,best}$ **[kg/km^3]**	**V**
A	$\Gamma_3 = 5.6633$	$\Gamma_3 = 5.1022$	−9.9%
	$\Gamma_5 = 7.6605$	$\Gamma_5 = 5.5256$	−27.8%
B	$\Gamma_3 = 5.4341$	$\Gamma_3 = 5.2798$	−2.8%
	$\Gamma_5 = 6.7110$	$\Gamma_5 = 6.1350$	−8.6%
C	$\Gamma_3 = 5.7421$	$\Gamma_3 = 5.5957$	−2.5%
	$\Gamma_5 = 8.0181$	$\Gamma_5 = 7.3684$	−8.1%

6. Conclusions

The presented results suggest that a unique AV has a deep effect on traffic dynamics, either in terms of emissions reduction or a decrease of concentrations for pollutants. Traffic waves are dampened, with a consequent positive impact on the amount of ozone and nitrogen oxides present at street level. Indeed, reductions for emissions and chemical species are not only due to the AV, but to the whole vehicle fleet,

as all vehicles along the ring road have smoother driving if autonomous capabilities reduce stop-and-go waves.

Controllers of three types were implemented: with infrastructure communication, with human-actuated information, and with local information. The first achieved the best performance, but the other two also had a significant impact.

Future research issues deal with different experiments to test the impact of AVs. The aim is to focus on the traffic instabilities in more complex scenarios dealing with the presence of more lanes, as well as habits of lane changing by drivers.

Author contributions

Conceptualization, B. P. and R. M.; methodology, M. B., B. P., R. M. and L.R.; software, M. B. and L. R.; validation, M. B., B. P., R. M. and L. R.; formal analysis, M. B., B. P., R. M. and L. R.; investigation, M. B., B. P., R. M. and L. R.; writing–original draft preparation, M. B., B. P., R. M. and L. R.; writing–review and editing, M. B., B. P., R. M. and L. R.; supervision, M. B., B. P., R. M. and L. R.; project administration, B. P. and R. M.

All authors have read and agreed to the published version of the manuscript.

Use of AI tools declaration

The authors declare they have not used Artificial Intelligence (AI) tools in the creation of this article.

Acknowledgments

Benedetto Piccoli is an editorial board member for Networks and Heterogeneous Media and was not involved in the editorial review or the decision to publish this article.

Conflict of interest

The authors declare there is no conflict of interest.

References

1. R. E. Stern, S. Cui, M. L. Delle Monache, R. Bhadani, M. Bunting, M. Churchill, et al., Dissipation of stop-and-go waves via control of autonomous vehicles: field experiments, *Transp. Res. Part C Emerg. Technol.*, **89** (2018), 205–221. https://doi.org/10.1016/j.trc.2018.02.005
2. R. E. Stern, Y. Chen, M. Churchill, F. Wu, M. L. Delle Monache, B. Piccoli, et al., Quantifying air quality benefits resulting from few autonomous vehicles stabilizing traffic, *Transport Res D-tr E*, **67** (2019), 351–365. https://doi.org/10.1016/j.trd.2018.12.008
3. J. J. LaMondia, D. J. Fagnant, H. Qu, J. Barrett, K. Kockelman, Shifts in long-distance travel mode due to automated vehicles: statewide mode-shift simulation experiment and travel survey analysis, *Transport. Res. Rec*, **2566** (2016), 1–11. https://doi.org/10.3141/2566-01

4. Y. Sugiyama, M. Fukui, M. Kikuchi, K. Hasebe, A. Nakayama, K. Nishinari, et al., Traffic jams without bottlenecks—experimental evidence for the physical mechanism of the formation of a jam, *New J. Phys.*, **10** (2008), 033001. https://doi.org/10.1088/1367-2630/10/3/033001

5. S. Tadaki, M. Kikuchi, M. Fukui, A. Nakayama, K. Nishinari, A. Shibata, et al., Phase transition in traffic jam experiment on a circuit, *New J. Phys.*, **15** (2013), 103034. https://doi.org/10.1088/1367-2630/15/10/103034

6. F. Wu, R. E. Stern, S. Cui, M. L. Delle Monache, R. Bhadani, M. Bunting, et al., Tracking vehicle trajectories and fuel rates in phantom traffic jams: Methodology and data, *Transport Res C-emer*, **99** (2019), 82–109. https://doi.org/10.1016/j.trc.2018.12.012

7. J. Liu, K. Kockelman, A. Nichols, Anticipating the emissions impacts of autonomous vehicles using the MOVES model, *Proceedings of the 95th Transportation Research Board Annual Meeting,* Washington, 2017.

8. O. Servin, K. Boriboonsomsin, M. Barth, An energy and emissions impact evaluation of intelligent speed adaptation, *Proceedings of the IEEE Intelligent Transportation Systems Conference (ITSC)*, (2006), 1257–1262. http://dx.doi.org/10.1109/ITSC.2006.1707395

9. F. Schäfer, R. Van Basshuysen, *Reduced emissions and fuel consumption in automobile engines*, Springer Science & Business Media, Berlin, 2013.

10. G. Fontaras, P. Pistikopoulos, Z. Samaras, Experimental evaluation of hybrid vehicle fuel economy and pollutant emissions over real-world simulation driving cycles, *Atmos. Environ.*, **42** (2008), 4023–4035. https://doi.org/10.1016/j.atmosenv.2008.01.053

11. K. Boriboonsomsin, M. J. Barth, W. Zhu, A. Vu, Eco-routing navigation system based on multisource historical and real-time traffic information, *IEEE trans Intell Transp Syst*, **13** (2012), 1694–1704. https://doi.org/10.1109/TITS.2012.2204051

12. L. Chapman, Transport and climate change: a review, *J Transp Geogr*, **15** (2007), 354–367. https://doi.org/10.1016/j.jtrangeo.2006.11.008

13. M. Barth, K. Boriboonsomsin, Real-world carbon dioxide impacts of traffic congestion, *Transp Res Rec*, **2058** (2008), 163–171. https://doi.org/10.3141/2058-20

14. F. An, M. Barth, J. Norbeck, M. Ross, Development of comprehensive modal emissions model: operating under hot-stabilized conditions, *Transp Res Rec*, **1587** (1997), 52–62. https://doi.org/10.3141/1587-07

15. D. Schuetzle, Sampling of vehicle emissions for chemical analysis and biological testing, *Environ. Health Perspect.*, **47** (1983), 65–80. https://doi.org/10.1289/ehp.834765

16. M. André, M. Keller, A. Sjödin, M. Gadrat, I. Mc Crae, P. Dilara, The artemis european tools for estimating the transport pollutant emissions, *Proceedings of the 18th International Emission Inventories Conference*, (2009), 1–10.

17. A. Cappiello, I. Chabini, E. K. Nam, A. Lue, M. A. Zeid, A statistical model of vehicle emissions and fuel consumption, *Proceedings of the 5th IEEE International Conference on Intelligent Transportation Systems (ITSC)*, (2002), 801–809. https://doi.org/10.1109/ITSC.2002.1041322

18. H. Teng, L. Yu, Y. Qi, Statistical microscale emission models incorporating acceleration and deceleration, *Proceedings of the 81st Transportation Research Board Annual Meeting*, (2010), 29.

19. L. I. Panis, S. Broekx, R. Liu, Modelling instantaneous traffic emission and the influence of traffic speed limits, *Sci. Total. Environ.*, **371** (2006), 270–285. https://doi.org/10.1016/j.scitotenv.2006.08.017

20. Y. Zhao, A. W. Sadek, Computationally-efficient approaches to integrating the MOVES emissions model with traffic simulators, *Procedia Comput. Sci.* , **19** (2013), 882–887. https://doi.org/10.1016/j.procs.2013.06.118

21. C. Balzotti, M. Briani, Estimate of traffic emissions through multiscale second order models with heterogeneous data, *Netw. Heterog. Media*, **17** (2022), 863–892. https://doi.org/10.3934/nhm.2022030

22. C. Balzotti, M. Briani, B. De Filippo, B. Piccoli, Towards a Comprehensive Model for the Impact of Traffic Patterns on Air Pollution, *Proceedings of the 6th International Conference on Vehicle Technology and Intelligent Transport Systems (VEHITS2020)*, **1** (2020), 221–228. https://doi.org/10.5220/0009391502210228

23. C. Balzotti, M. Briani, B. De Filippo, B. Piccoli, A computational modular approach to evaluate NO_x emissions and ozone production due to vehicular traffic, *Discrete Cont Dyn-B*, **27** (2022), 3455–3486. https://doi.org/10.3934/dcdsb.2021192

24. S. Cui, B. Seibold, R. E. Stern, D. B. Work, Stabilizing traffic flow via a single autonomous vehicle: Possibilities and limitations, *2017 IEEE Intelligent Vehicle Symposium (IV)*, (2017), 1336–1341. https://doi.org/10.1109/IVS.2017.7995897

25. J. H. Seinfeld, S. N. Pandis, *Atmospheric Chemistry and Physics: From Air Pollution to Climate Change*, John Wiley & Sons, New York, 2016.

26. R. P. Wayne, *Chemistry of Atmospheres*, Clarendon Press, Oxford, 1991.

27. D. J. Jacob, Heterogeneous chemistry and troposheric ozone, *Atmos. Environ.*, **34** (2000), 2131–2159. https://doi.org/10.1016/S1352-2310(99)00462-8

28. F. Song, J. Y. Shin, R. Jusino-Atresino, Y. Gao, Relationships among the springtime ground-level NO_x, O_3 and NO_3 in the vicinity of highways in the US East Coast, *Atmospheric Pollut. Res.*, **2** (2011), 374–383. https://doi.org/10.5094/APR.2011.042

29. R. Smit, L. Ntziachristos, P. Boulter, Validation of road vehicle and traffic emission models–A review and meta-analysis, *Atmos. Environ.*, **44** (2010), 2943–2953. https://doi.org/10.1016/j.atmosenv.2010.05.022

30. S. Manahan, *Environmental Chemistry*, CRC press, Boca Raton, 2017. https://doi.org/10.1201/9781315160474

31. H. Omidvarborna, A. Kumar, D. S. Kim, NO_x emissions from low-temperature combustion of biodiesel made of various feedstocks and blends, *Fuel Process. Technol.*, **140** (2015), 113–118. https://doi.org/10.1016/j.fuproc.2015.08.031

32. R. Atkinson, W. P. L. Carter, Kinetics and mechanisms of the gas-phase reactions of ozone with organic compounds under atmospheric conditions, *Chem. Rev.*, **84** (1984), 437–470. https://doi.org/10.1021/cr00063a002
33. M. Rößler, T. Koch, C. Janzer, M. Olzmann, Mechanisms of the NO_2 formation in diesel engines, *MTZ Worldw.*, **78** (2017), 70–75. https://doi.org/10.1007/s38313-017-0057-2
34. D. C. Carslaw, S. D. Beevers, J. E. Tate, E. J. Westmoreland, M. L. Williams, Recent evidence concerning higher NO_x emissions from passenger cars and light duty vehicles, *Atmos. Environ.*, **45** (2011), 7053–7063. https://doi.org/10.1016/j.atmosenv.2011.09.063
35. M. Z. Jacobson, *Fundamentals of Atmospheric Modeling*, Cambridge University Press, Cambridge, 2005. https://doi.org/10.1017/CBO9781139165389
36. E. Hairer, G. Wanner, *Solving Ordinary Differential Equations II. Stiff and Differential-Algebraic Problem, Second edition*, Springer Berlin Heidelberg, New York, 1996.
37. M. Garavello, K. Han, B. Piccoli, Models for vehicular traffic on networks, *Applied Mathematics Vol. 9*, American Institute of Mathematical Sciences, Springfield, 2016.
38. M. J. Lighthill, G. B. Whitham, On kinematic waves II. A theory of traffic flow on long crowded roads, *P. ROY SOC A-MATH PHY*, **229** (1955), 317–345. https://doi.org/10.1098/rspa.1955.0089
39. P. I. Richards, Shock Waves on the Highway, *Oper. Res.*, **4** (1956), 42–51. https://doi.org/10.1287/opre.4.1.42
40. S. Albeaik, A. Bayen, M. T. Chiri, X. Gong, A. Hayat, N. Kardous, et al., Limitations and improvements of the intelligent driver model (IDM), *SIAM J. Appl. Dyn. Syst.*, **21** (2022), 1862–1892. https://doi.org/10.1137/21M1406477
41. B. Piccoli, K. Han, T. L. Friesz, T. Yao, J. Tang, Second-order models and traffic data from mobile sensors, *Transp Res Part C Emerg Technol*, **52** (2015), 32–56. https://doi.org/10.1016/j.trc.2014.12.013
42. R. A. Ramadan, B. Seibold, *Traffic flow control and fuel consumption reduction via moving bottlenecks*, arXiv:1702.07995, [Preprint], (2017) [cited 2024 August 22]. Available from: https://doi.org/10.48550/arXiv.1702.07995
43. R. M. Colombo, P. Goatin, E. Rossi, *A Hyperbolic-Parabolic framework to manage traffic generated pollution*, hal-04504572, [Preprint], (2024) [cited 2024 August 22]. Available from: https://hal.science/hal-04504572

AIMS Press